

ORIGINAL ARTICLE

Cellular senescence primes liver fibrosis regression through Notch-EZH2

Ping Song[#] | Juan-Li Duan[#] | Jian Ding[#] | Jing-Jing Liu | Zhi-Qiang Fang |
Hao Xu | Zhi-Wen Li | Wei Du | Ming Xu | Yu-Wei Ling | Fei He |
Kai-Shan Tao* | Lin Wang* 

Department of Hepatobiliary Surgery,
Xi-Jing Hospital, Fourth Military Medical
University, Xi'an, China

***Correspondence**

Lin Wang and Kai-Shan Tao, Department
of Hepatobiliary Surgery, Xi-Jing Hospital,
Fourth Military Medical University, Xi'an
710032, China.

Email: fierywang@163.com and
taokaishan0686@163.com

Funding information

National Key Research and Development
Program of China, Grant/Award
Numbers: 2021YFA1100500,
2016YFA0102100; National Natural
Science Foundation of China,
Grant/Award Numbers: 81422009,
81770560, 82325007

Abstract

Cellular senescence plays a pivotal role in wound healing. At the initiation of liver fibrosis regression, accumulated senescent cells were detected and genes of senescence were upregulated. Flow cytometry combined with single-cell RNA sequencing analyses revealed that most of senescent cells were liver nonparenchymal cells. Removing senescent cells by dasatinib and quercetin (DQ), alleviated hepatic cellular senescence, impeded fibrosis regression, and disrupted liver sinusoids. Clearance of senescent cells not only decreased senescent macrophages but also shrank the proportion of anti-inflammatory M2 macrophages through apoptotic pathway. Subsequently, macrophages were depleted by clodronate, which diminished hepatic senescent cells and impaired fibrosis regression. Mechanistically, the change of the epigenetic regulator enhancer of zeste homolog2 (EZH2) accompanied with the emergence of hepatic senescent cells while liver fibrosis regressed. Blocking EZH2 signaling by EPZ6438 reduced hepatic senescent cells and macrophages, decelerating liver fibrosis regression. Moreover, the promoter region of EZH2 was transcriptionally suppressed by Notch-Hes1 (hairy and enhancer of split 1) signaling. Disruption of Notch in macrophages using *Lyz2* (lysozyme 2)^{Cre}-RBP-J (recombination signal binding protein J κ)^{f/f} transgenic mice, enhanced hepatic cellular senescence, and facilitated fibrosis regression by upregulating EZH2 and blocking EZH2 abrogated the above effects caused by Notch deficiency. Ultimately, adopting Notch inhibitor Ly3039478 or exosome-mediated RBP-J decoy oligodeoxynucleotides accelerated liver fibrosis regression by augmenting hepatic cellular senescence.

KEYWORDS

EZH2, liver fibrosis regression, macrophage, Notch, senescence

[#]Ping Song, Juan-Li Duan, and Jian Ding contributed equally to this study.

This is an open access article under the terms of the [Creative Commons Attribution](https://creativecommons.org/licenses/by/4.0/) License, which permits use, distribution and reproduction in any medium, provided the original work is properly cited.

© 2023 The Authors. *MedComm* published by Sichuan International Medical Exchange & Promotion Association (SCIMEA) and John Wiley & Sons Australia, Ltd.

1 | INTRODUCTION

Chronic liver injuries lead to liver fibrosis, by activating hepatic extracellular matrix-derived myofibroblasts.¹ When the causative injuries are removed, clinical and experimental liver fibrosis may regress.^{1,2} Hepatocytes, hepatic stellate cells (HSCs), liver sinusoidal endothelial cells (LSECs), and immune cells, particularly macrophages, cooperate to initiate the regression of liver fibrosis.³⁻⁵ Accumulated investigations focus mainly on the progression of liver fibrosis; however, fibrosis regression is relatively understudied.⁶ To investigate the underlying mechanisms of regression, a new therapeutic strategy may be established to treat liver fibrosis.⁷

Cellular senescence is a permanent state of cell cycle arrest.⁸ Pathways of P16^{Ink4a} and P53/P21, which are important for irreversible growth arrest, have been widely recognized as regulators for cellular senescence.⁹ Senescent cells not only originate from age-related diseases,¹⁰ but also emerge in tumor suppression,¹¹ tissue remodeling,¹² wound healing,¹³ and protection against organ fibrosis.¹⁴ The coordinated induction of senescence benefits fibrotic scar removal through senescence-associated secretory phenotype (SASP).¹⁵ Hepatic stellate cell-derived senescence limited fibrogenesis¹⁵ and depletion of p16^{High} hepatic senescent cells accelerated fibrosis.¹⁶ However, misregulated senescence deteriorated organ remodeling. Application of senolytics to remove senescent cells, improved liver regeneration¹⁷ and ameliorated steatohepatitis.¹⁸ Recently, our group reported that shear stress-induced endothelial cellular senescence impaired liver regeneration following partial hepatectomy.¹⁹ Thus, the role of senescent cells in response to liver injury is still controversial.

EZH2 is a histone H3K27me3 methyltransferase.²⁰ EZH2 usually functions as an epigenetic regulator of cell cycle,²¹ autophagy,²² apoptosis,²³ and DNA damage repair.²⁴ Numerous studies have identified the regulatory role of EZH2 in many diseases,²⁵ including cancer.^{26,27} As the change of the expression of epigenetic genes is associated with senescence-induced phenotype,²⁸ the importance of EZH2 in driving cellular senescence attracts our interests. P21 is known as a landmark gene of senescence.²⁹ EZH2 can directly bind to the promoter region of P21 and facilitate H3K27me3 modification to orchestrate senescence.³⁰ Although our previous findings proved that shear stress-induced cellular senescence was accompanied with the upregulation of EZH2 at the late phase of liver regeneration,¹⁹ the detailed regulatory role of EZH2 in manipulating liver injury-induced senescence was not fully elucidated. Therefore, we selected EZH2 as a

key molecule in the regulation of senescence. In this study, we found that EZH2 was transcriptionally suppressed by Hes1, a direct downstream gene of Notch signaling.³¹ Once RBP-J, the main transcriptional mediator of Notch,³² was disrupted, the effect of EZH2-regulated senescence could be reversed. The potential link between Notch and EZH2 unveils a brand new mechanism in the regulation of cellular senescence.

In this study, we found that EZH2-regulated senescent cells accumulated while liver fibrosis regression began. Disruption of the epigenetic regulation of EZH2 removed anti-inflammatory senescent cells and impaired fibrosis regression. As the transcription of EZH2 was impeded by Notch-Hes1 signaling, blocking Notch facilitated fibrosis regression by strengthening EZH2-regulated senescence, providing a promising therapeutic approach for the management of liver fibrosis.

2 | RESULTS

2.1 | Accumulated senescent cells emerge at the beginning of liver fibrosis regression

Liver fibrosis was induced by 6-week CCl₄ (carbon tetrachloride) injection.³³ To evaluate fibrosis regression, mice were sacrificed and analyzed on 1, 2, 3, 4, 5, 7, or 14 days following the removal of CCl₄. An increase of liver/body weight ratio was found on day 3 of regression (Figure S1A). Serum ALT and AST levels peaked on day 1 and declined subsequently on day 3 (Figure S1B), which was consistent with the change of Masson staining (Figure S1C,D). As shown by the immunofluorescent (IF) and IHC (immunohistochemistry) staining (Figure 1A and Figure S1E), fibrosis-associated markers like Desmin and Masson significantly decreased on day 3, while SM22 (smooth muscle 22) and α SMA (alpha smooth muscle actin) declined on days 5 and 7, respectively, after CCl₄ withdrawal, confirming the resolution of liver fibrosis. SA- β -gal (senescence-associated β -galactosidase) is the most commonly utilized marker for identifying senescent cells.³⁴ Interestingly, the maximum level of SA- β -gal staining was observed 3 days after CCl₄ withdrawal (Figure 1B). Additionally, RT-qPCR (real-time quantitative PCR) analyses of primary macrophages revealed an upregulation in terms of gene expression related to senescence, including P16, P21, and P53 on day 3 of regression (Figure 1C). Western blotting (WB) quantification showed that protein levels of P16, P21, and P53 peaked on day 3 of regression (Figure 1D). These data collectively proved that cellular senescence emerged at the beginning of fibrosis regression.

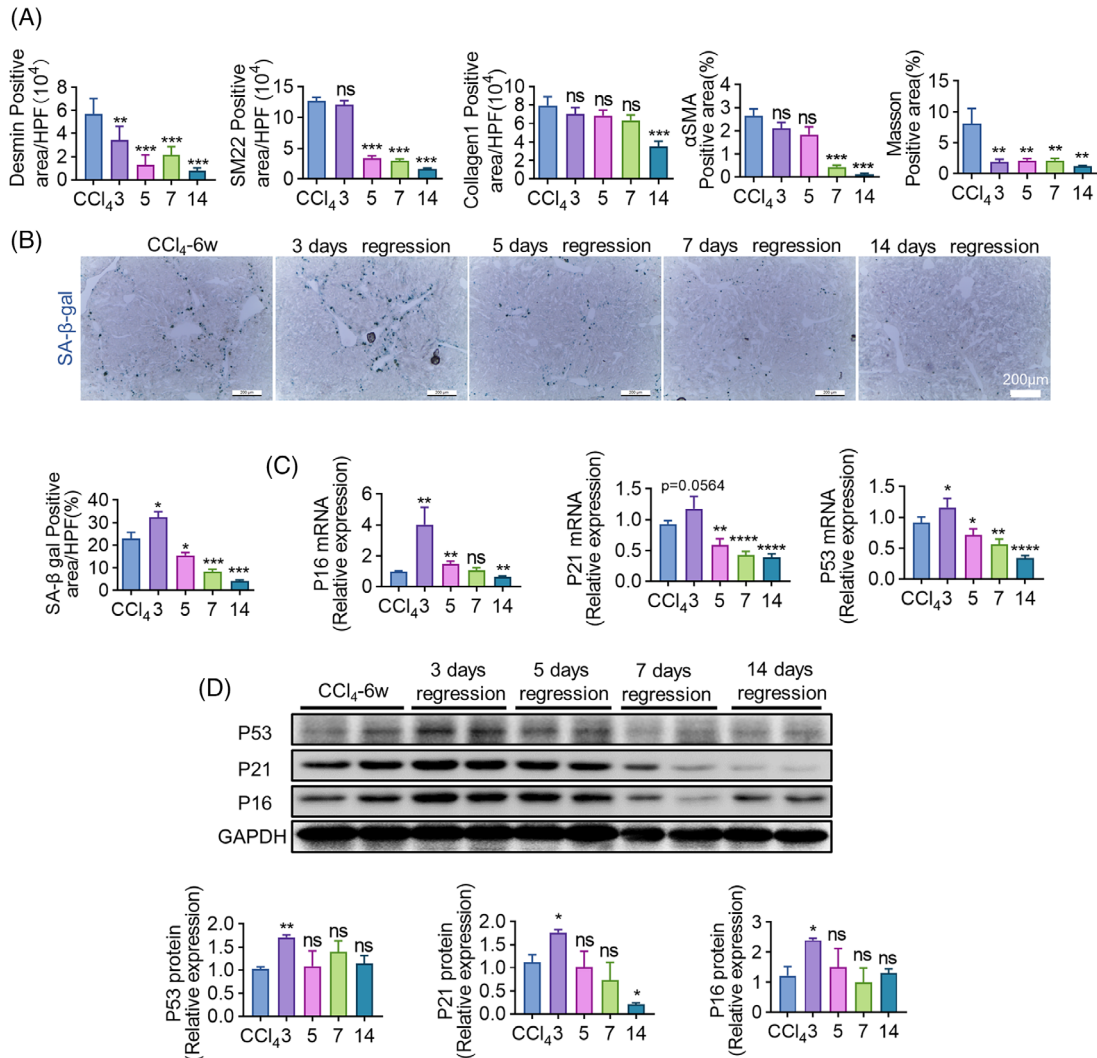


FIGURE 1 The emergence of accumulated senescent cells during fibrosis regression. (A) The quantification of positive areas of IF (Desmin, SM22, Collagen1) and IHC (α SMA, Masson) staining of livers on days 3, 5, 7, and day 14 of regression. Mice sacrificed immediately after the 12th CCl₄ injection served as control. (B) Frozen sections of livers were stained with a Senescence β -galactosidase Staining Kit (SA- β -gal Kit). Positive areas of SA- β -gal were quantitatively compared. (C) Relative mRNA expressions of senescence-related molecules including P16, P21, and P53 in isolated macrophages were determined using RT-qPCR during the regression of liver fibrosis; β -actin gene was used as an internal reference. (D) WB analyses of P16, P21, and P53 expression of isolated macrophages at various time points of regression; GAPDH served as an internal control. Bars = means \pm SD; $n = 2-4$; * $p < 0.05$, ** $p < 0.01$, *** $p < 0.001$, **** $p < 0.0001$; ns, not significant.

2.2 | Senescent cells predominantly originate from liver nonparenchymal cells

Next, we try to clarify the origin of the senescent cells. Flow cytometry (FCM) demonstrated that a significant increase of SA- β -gal⁺ senescent cells on regression day 3 could be detected in liver nonparenchymal cells (NPCs) (from 0.455% to 0.842%) but not hepatocytes (Figure 2A). Further analyses revealed that 44.74% of senescent cells were F4/80⁺ KCs (Kupffer cells), 40.60% were VEGFR2⁺ LSECs, and 20.69% were Desmin⁺ HSCs (Figure 2B). These FCM data proved that senescent cells dominantly originated from liver NPCs, especially KCs and LSECs. To confirm

these findings, scRNA-seq (single-cell RNA sequence) was manipulated in mice with fibrosis regression. The distribution of different hepatic cells and P16⁺ senescent cells is shown in Figure 2C,D. The gene set enrichment analysis (GSEA) and gene set variation analysis (GSVA) identified that senescence marker genes, which enriched in livers with fibrosis regression, mostly expressed in KCs, BMDM (bone marrow-derived macrophages), MFs (myofibroblasts), and LSECs (Figure 2G,H). We then compared the expression of marker genes of senescence between control and experimental mice by scRNA-seq. The upregulation of P16 and P21 expression was observed in hepatic cells of mice with fibrosis regression (Figure 2E).

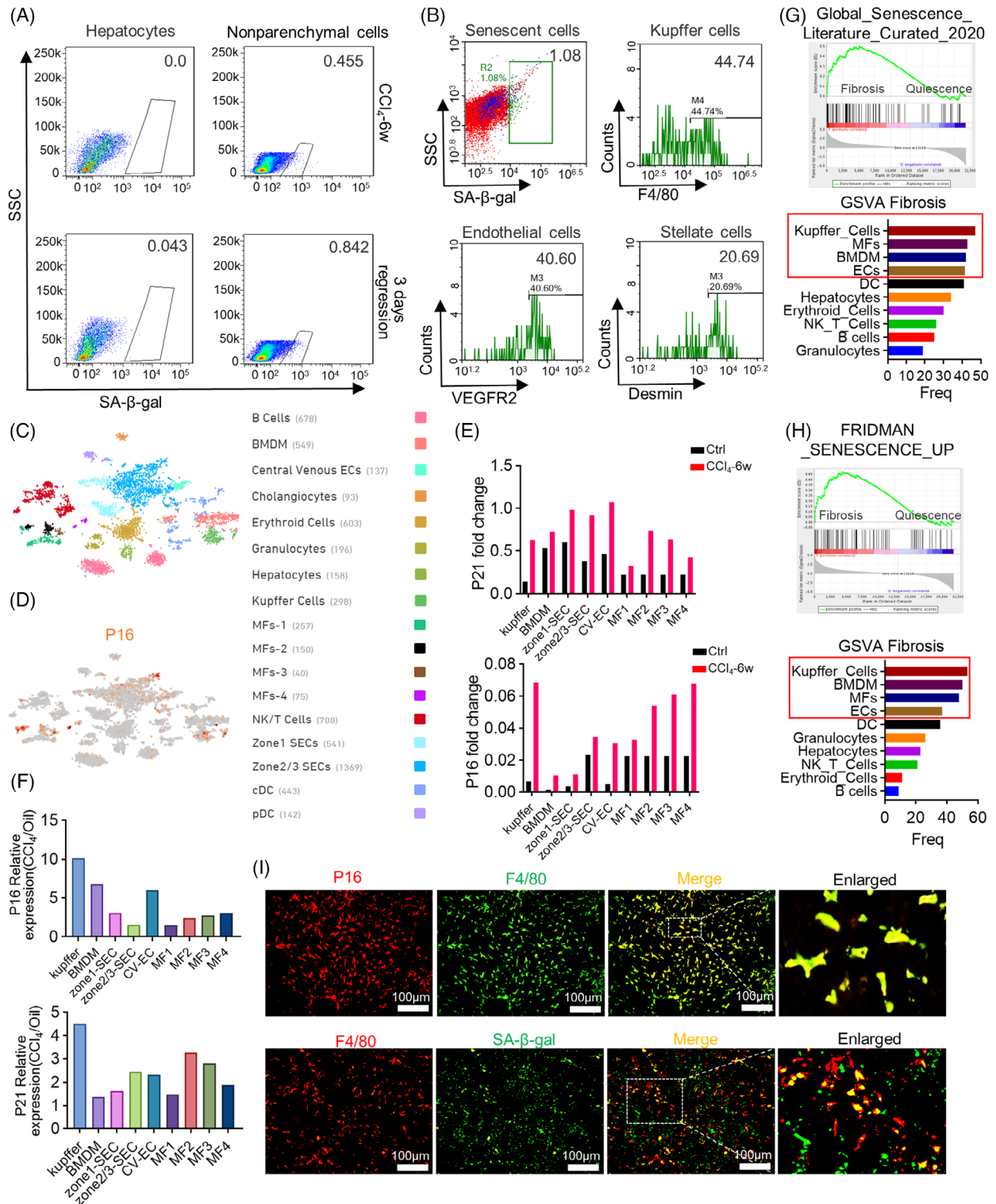


FIGURE 2 Identification of the origin of senescent cells. (A) Single-cell suspensions collected from hepatocytes or liver NPCs were analyzed by FCM 3 days after the withdrawal of CCl₄; $n = 1$. (B) FCM analyses showed the proportion of KCs (F4/80), LSECs (VEGFR2), and HSCs (desmin) in senescent NPCs (SA- β -gal) on regression day 3. (C) tSNE (t-distributed stochastic neighboring embedding) clustering representation of the distinct cell types of liver NPCs following CCl₄ toxicity. (D) Gene expression of P16 was visualized by tSNE feature plots. (E and F) Fold change in expression of P16 and P21 observed in individual cell types by scRNA-seq. (G and H) GSEA analyses with Global Senescence Literature Curated 2020 or Fridman Senescence UP in mice with CCl₄ removal and control mice. GSEA enrichment score was performed for the above two senescence-related gene sets of both experimental and control mice, bar graphs represented the frequency basis of positive cells in various NPC types by GSEA score. (I) IF co-staining of P16 (red)/F4/80 (green) or SA- β -gal (green)/f4/80 (red) of livers on regression day 3. Scale bar: 100 μ m. Bars = means \pm SD; $n = 3$.

However, the biggest alteration of P16 and P21 could be found in KCs (Figure 2F). Additionally, IF staining confirmed the co-stain of macrophages (F4/80⁺) and senescent cells (P16⁺ or SA- β -gal⁺) on regression day 3 (Figure 2I). Collectively, these findings preliminarily implied that hepatic macrophages devoted major contribution to the emergence of cellular senescence.

2.3 | Depletion of senescent cells inhibits liver fibrosis regression and disrupts hepatic sinusoids

Subsequently, DQ which is one of the classical senolytics,³⁵ was intragastric administration on regression day 0.5 and day 2.5 to remove senescent cells. Mice were analyzed on day 3 as previously (Figure 3A). After DQ administration, both serum ALT (alanine aminotransferase) and AST (aspartate aminotransferase) levels increased (Figure 3B), implying the liver function deteriorated after senescent cell depletion. WB (Figure 3C,D) and RT-qPCR (Figure 3E) analyses confirmed the downregulation of senescence markers, including P16, P21, and P53. SA- β -gal staining also reflected the successful removal of senescent cells (Figure 3F). Next, we observed the change of liver fibrosis. Apparently, α SMA, Sirius red, collagen1, and desmin staining all illustrated that liver fibrosis was aggravated by DQ (Figure 3G), indicating removing senescent cells reversed fibrosis regression.

Besides, enhanced laminin stain and reduced LSEC fenestration, which were determined by IF staining and SEM (scanning electronic microscopy), respectively, confirmed the capillarization of liver sinusoids (Figure 3H). To assess alterations in blood flow within sinusoids, fluorescent polystyrene microspheres were injected into the spleen and subsequently detected within the liver. Bioluminescence imaging analysis showed enhanced liver fluorescence after DQ treatment (Figure 3I). Furthermore, increased fluorescent microspheres were detected in livers of mice with DQ administration (Figure 3J). These results implied that liver sinusoids were occluded once senescent cells were removed.

2.4 | Removing senescent cells diminishes anti-inflammatory macrophages through apoptotic pathway

We then try to clarify how senescent cells facilitate liver fibrosis regression. According to IF staining, P21⁺ or γ -H2AX⁺ senescent macrophages were greatly reduced by DQ on regression day 3 (Figure 4A). FCM analyses also confirmed the decrease of macrophage senescence (from

57.0% to 35.1%) after DQ administration (Figure 4B), which proved that hepatic macrophages attributed to the emergence of senescence. Besides, total macrophages of livers treated with DQ decreased significantly (Figure 4C). As we know, macrophages usually stimulate liver fibrosis in different models.³⁶ However, our findings showed that depletion of senescent cells decreased hepatic macrophages and impedes fibrosis regression. To illustrate this contradiction, FCM analyses were performed in hepatic macrophages between control and DQ-treated mice. As shown in Figure 4D, DQ removed F4/80⁺CD11b⁺ hepatic macrophages majorly through reducing M2 (from 31.7% to 20.4%), but not M1 macrophages. Marker genes of M2 macrophages like ARG (arginase), IL-10 (interleukin-10), MR (mannose receptor c-type 1), and YM-1 (chitinase-like 3) were all downregulated by DQ, which were determined by RT-qPCR (Figure 4E). As M2 macrophages normally take anti-inflammatory effects,³⁷ we then evaluated the change of anti-inflammatory macrophages following DQ administration. As expected, DQ significantly lowered the percentage of Ly6c^{Low} macrophages (from 45.5% to 24.5%) (Figure 4F), which have been widely accepted as anti-inflammatory macrophages.³⁸ Thus, we may conclude that most of senescent macrophages induced by fibrosis regression were anti-inflammatory macrophages.

We then explored the involved mechanism of the reduction of anti-inflammatory macrophages caused by DQ. Apoptotic liver cells increased after DQ injection, which was determined by TUNEL (terminal deoxynucleotidyl transferase-mediated dUTP nick-end labeling) staining (Figure 4G). Besides, TUNEL and F4/80 co-stain (Figure 4H) and anti-Annexin V FCM analyses (Figure 4I) both revealed that apoptotic liver macrophages significantly increased once senescent cells were removed. Mechanistically, apoptosis-associated pathways, such as cleaved caspase 3 and BAX were upregulated by DQ in both protein (Figure 4J) and mRNA levels (Figure 4K), suggesting DQ diminished anti-inflammatory macrophages through apoptotic pathways. In summary, DQ prevented the fibrosis regression by reducing the anti-inflammatory macrophages through apoptotic pathways.

2.5 | Clearance of macrophages alleviates cellular senescence and impedes liver fibrosis regression

To confirm that senescent cells initiate fibrosis regression through anti-inflammatory macrophages, we then removed macrophages to evaluate the change of regression. Clodronate injected Intraperitoneally (IP) on regression day 0.5 and day 2.5 (Figure 5A), increased the liver/body weight ratio of mice analyzed on day 3

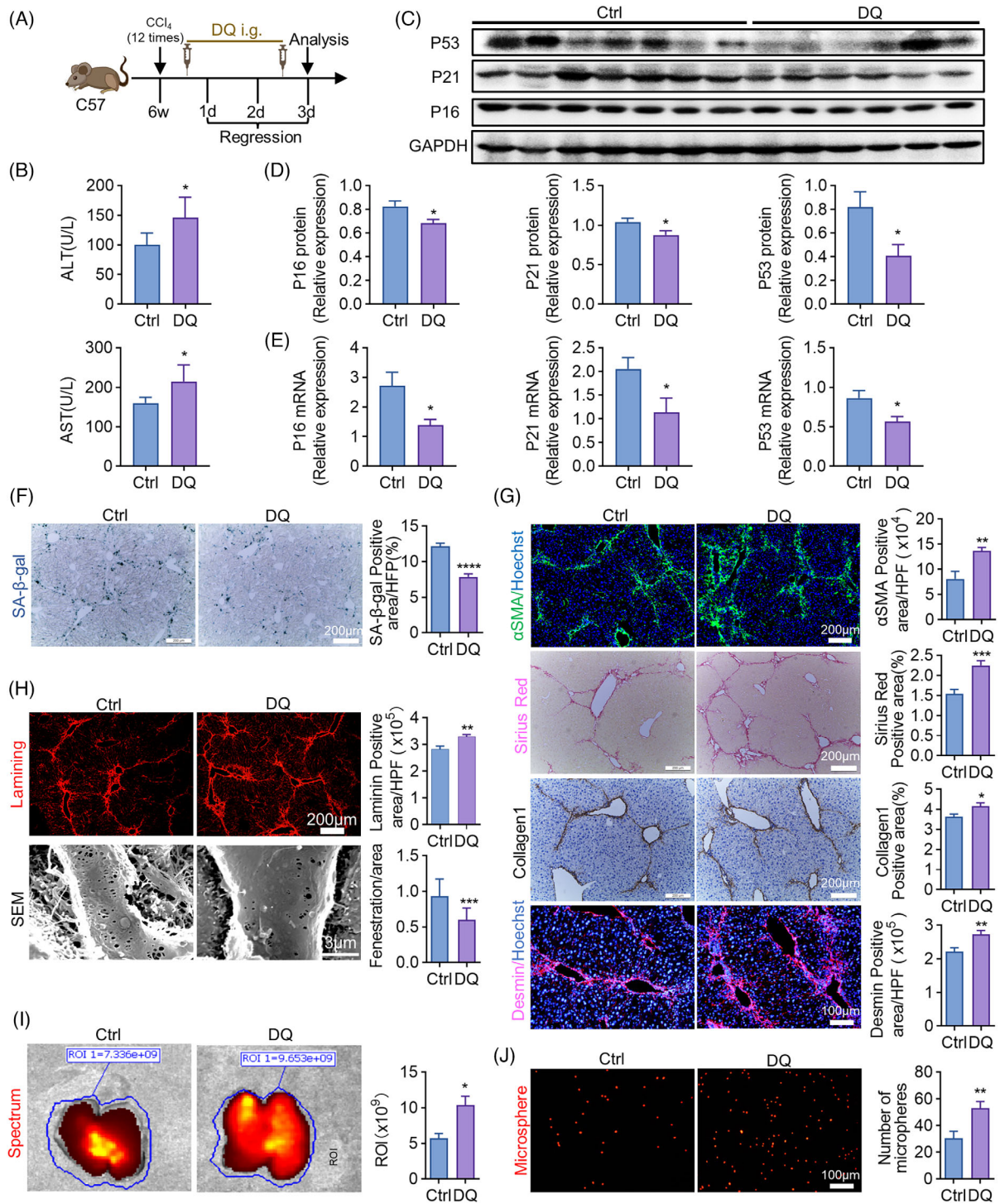


FIGURE 3 Removing senescent cells inhibits liver fibrosis regression. (A) The strategy of DQ (dasatinib and quercetin) administration during the regression of liver fibrosis. All the experimental mice were sacrificed and analyzed on regression day 3. The cartoon was created by Photoshop. i.g. means oral gavage. (B) Detection of serum ALT, AST in DQ-treated and control mice. (C) WB analyses of P16, P21, and P53 expressions in KCs of DQ-treated and control mice; GAPDH served as an internal reference. (D) The quantification of (C). (E) The mRNA levels of P16, P21, and P53 were detected by RT-qPCR in DQ-treated and control mice; β -actin was used as an internal reference. (F) Liver sections collected from DQ-treated and control mice were stained by SA- β -gal staining kit. SA- β -gal-positive cells were quantitatively compared. Scale bar: 200 μm . (G) IF (α SMA, Desmin) and IHC (Sirius red, Collagen1) staining of DQ-treated and control mice. Positive areas were quantified and compared. Scale bar: 200 μm (α SMA, Sirius red, Collagen1), scale bar: 100 μm (desmin). (H) Staining of Laminin in DQ-treated and control mice. Positive areas were quantitatively compared. Scale bar: 200 μm . Sinusoidal fenestrations were examined and quantitatively compared by SEM in DQ-treated and control mice. Scale bar: 3 μm . (I and J) Red fluorescent microspheres injected into the spleen were subsequently observed in the liver. The fluorescence intensity was compared in (I) and the microspheres were quantified in (J). Scale bar: 100 μm . Bars = means \pm SD; $n = 6$; * $p < 0.05$, ** $p < 0.01$, **** $p < 0.0001$.

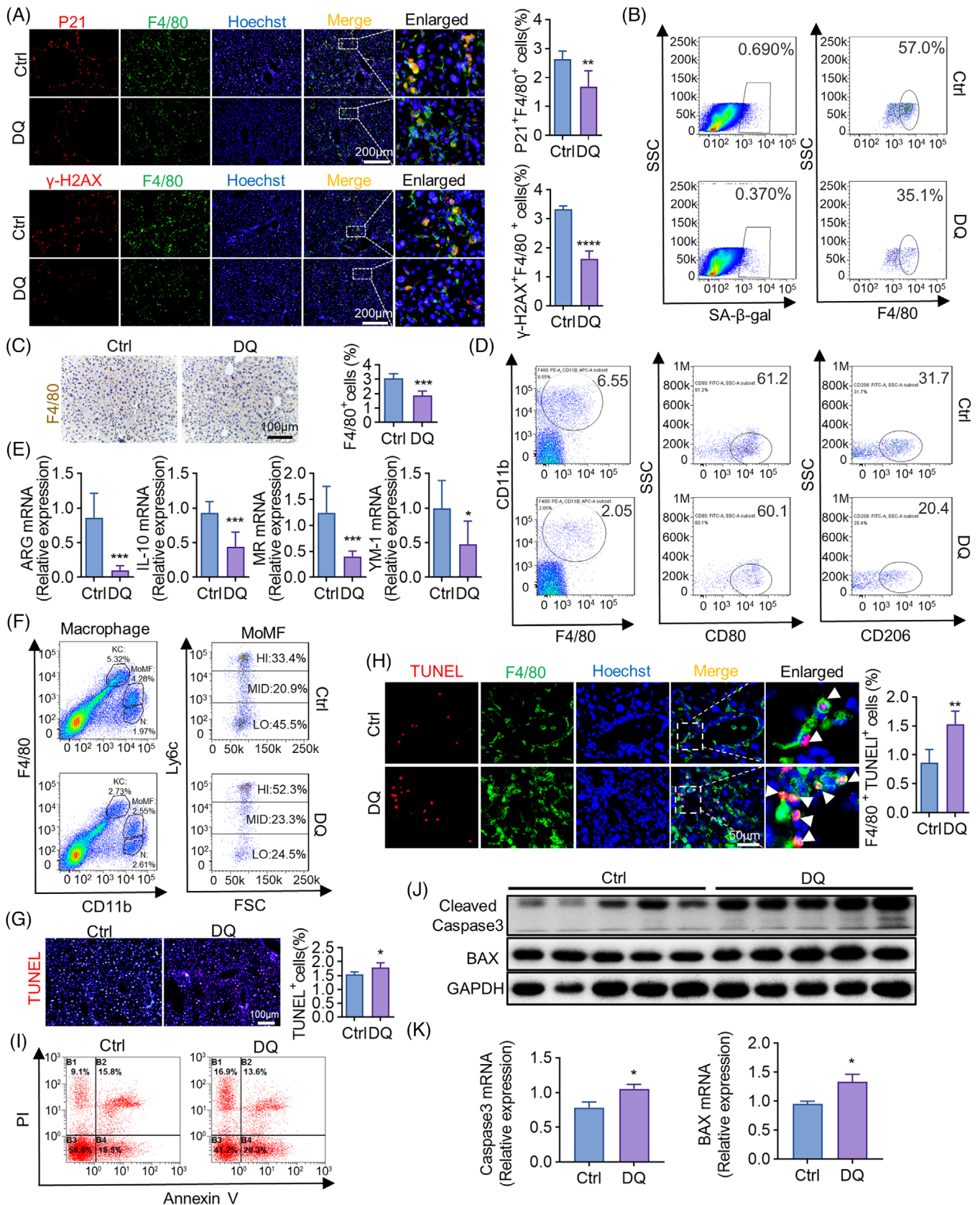


FIGURE 4 Clearance of senescent cells diminishes M2 macrophages. All the experimental mice were sacrificed and analyzed on regression day 3. (A) IF co-staining of F4/80 (green) and P21 (red) or γ -H2AX (red)/f4/80 (green) in livers of DQ-treated and control mice. Double positive cells were quantitatively compared. Scale bar: 200 μ m. (B) The proportion of SA- β -gal⁺ or F4/80⁺ cells in liver NPCs of DQ-treated and control mice was analyzed by FCM. (C) Liver sections collected from DQ-treated and control mice were analyzed using

(Figure 5B). Serum AST and ALT levels were elevated in clodronate-treated group (Figure 5C). IF staining of F4/80 proved the successful clearance of hepatic macrophages (Figure 5E). FCM analyses further confirmed the decrease of KCs (from 5.08% to 0.55%) and senescent macrophages (from 0.50% to 0.38%) in livers of clodronate-treated mice (Figure 5D). Importantly, the expression of marker genes of senescence, such as P16 and P21, were downregulated by clodronate in both protein (Figure 5F) and mRNA levels (Figure 5G). SA- β -gal staining also showed that removing macrophages diminished hepatic cellular senescence (Figure 5H). Next, Desmin and α SMA IF staining performed in livers of control and clodronate-treated mice showed that depletion of macrophages impeded fibrosis regression (Figure 5I). The expression of fibrosis-related genes like SM22, α SMA, and IL-1 β (interleukin-1 β) was downregulated by clodronate as well, which was determined by RT-qPCR (Figure 5J). Besides, reduced LSEC fenestration was observed in mice with clodronate administration (Figure 5K). These data implied that most of the macrophages removed by clodronate exerted anti-inflammatory effects during the process of regression.

2.6 | The epigenetic regulator EZH2 impels cellular senescence and promotes liver fibrosis regression

EZH2, an epigenetic modulator, has been regarded as a driver of cellular senescence.¹⁹ To illustrate the underlying mechanism, the expression of EZH2 was measured during the process of fibrosis regression. In consistent with the change of senescence (Figure 1B), the peaked expression of EZH2 occurred on day 3 as well, which was determined by WB (Figure 6A) and RT-qPCR (Figure 6B). We then evaluated EZH2 expression in livers with senescent cells or macrophages depletion. DQ and clodronate lowered EZH2 protein level (Figure 6C), and clodronate reduced the mRNA expression of EZH2 (Figure 6D), implying the possibility that DQ and clodronate inhibited senescence and regression through EZH2. To prove this hypothesis, EPZ6438, an inhibitor of EZH2, was adminis-

trated three doses during regression (Figure 6E). EPZ6438 increased relative liver weight (Figure 6F) and deteriorated liver function (Figure 6G). Besides, blocking EZH2 by EPZ6438 alleviated cellular senescence (Figure 6H,I), impaired fibrosis regression (Figure 6J,L), and reduced hepatic macrophages (Figure 6K). These findings collectively proved that EZH2-regulated senescence advanced liver fibrosis regression.

2.7 | Notch-Hes1 signaling impedes senescence-driven fibrosis regression by suppressing the transcription of EZH2

After analyzing the promoter region of EZH2, we discovered multiple putative binding sites for Hes1 transcription repressor (Figure 7A,B). ChIP (chromatin immunoprecipitation)-qPCR results demonstrated a significant binding affinity of Hes1 to the site3 and site4 of EZH2 promoter. Blockade of Notch signaling using GSI (gamma-secretase inhibitor)-treated macrophages further significantly inhibited this enrichment efficiency (Figure 7C,D), suggesting Hes1 inhibits EZH2 transcription by interacting with the EZH2 promoter region.

We then observed the regulatory effect of Notch-Hes1 signaling on cellular senescence. In the in vitro study, GSI, a classical Notch signaling inhibitor, significantly enhanced SA- β -gal⁺ stain (Figure 7E) and increased P16 and P21 mRNA levels (Figure 7F) in RAW264.7 macrophages. In the in vivo study, inactivation of macrophage-derived Notch signaling was achieved by constructing *Lyz2^{Cre}-RBP-J^{f/f}* transgenic mice as previously we did.³⁹ Disruption of Notch/RBP-J in macrophages, triggered hepatic cellular senescence (Figure 7G,H) and upregulated the mRNA level of EZH2 (Figure 7H). IF staining confirmed the increased EZH2 expression in livers of *Lyz2^{Cre}-RBP-J^{f/f}* mice (Figure 7I). These data implied that macrophage-derived Notch signaling deactivated senescence by impeding EZH2. During the process of fibrosis regression (Figure 7J), transgenic inactivation of Notch signaling decreased serum AST but

anti-F4/80 IHC. F4/80-positive cells were quantitatively compared. Scale bar: 100 μ m. (D) Isolated liver NPCs from DQ-treated or control mice were analyzed by FCM to detect the change of polarization (M1:CD80; M2:C206). (E) KCs were magnetically isolated from DQ-treated and control mice. Molecular markers of M2 macrophages were determined by RT-qPCR, with β -actin as an internal control. (F) Isolated liver NPCs from DQ-treated and control mice were analyzed by FCM to detect F4/80⁺CD11b⁺Ly6C^{hi} or F480⁺CD11b⁺Ly6C^{lo} proportions. MoMP, monocyte-derived macrophages; KC, Kupffer cells; N, neutrophils; HI, high; MID, middle; LO, low. (G and I) TUNEL staining and FCM were used to detect apoptotic liver cells in DQ-treated and control mice. TUNEL⁺ cells were quantitatively compared (G). Scale bar: 100 μ m. (H) IF co-staining of TUNEL (red) and F4/80 (green) in livers of DQ-treated and control mice. Double positive cells were quantitatively compared. Scale bar: 50 μ m. (J) Protein levels of cleaved caspase3 and BAX in KCs isolated from DQ-treated and control mice were determined by WB; GAPDH served as an internal control. (K) RT-qPCR analyses of cleaved caspase3 and BAX in KCs isolated from DQ-treated and control mice. Bars = means \pm SD; $n = 3-6$; * $p < 0.05$, ** $p < 0.01$, *** $p < 0.001$, **** $p < 0.0001$.

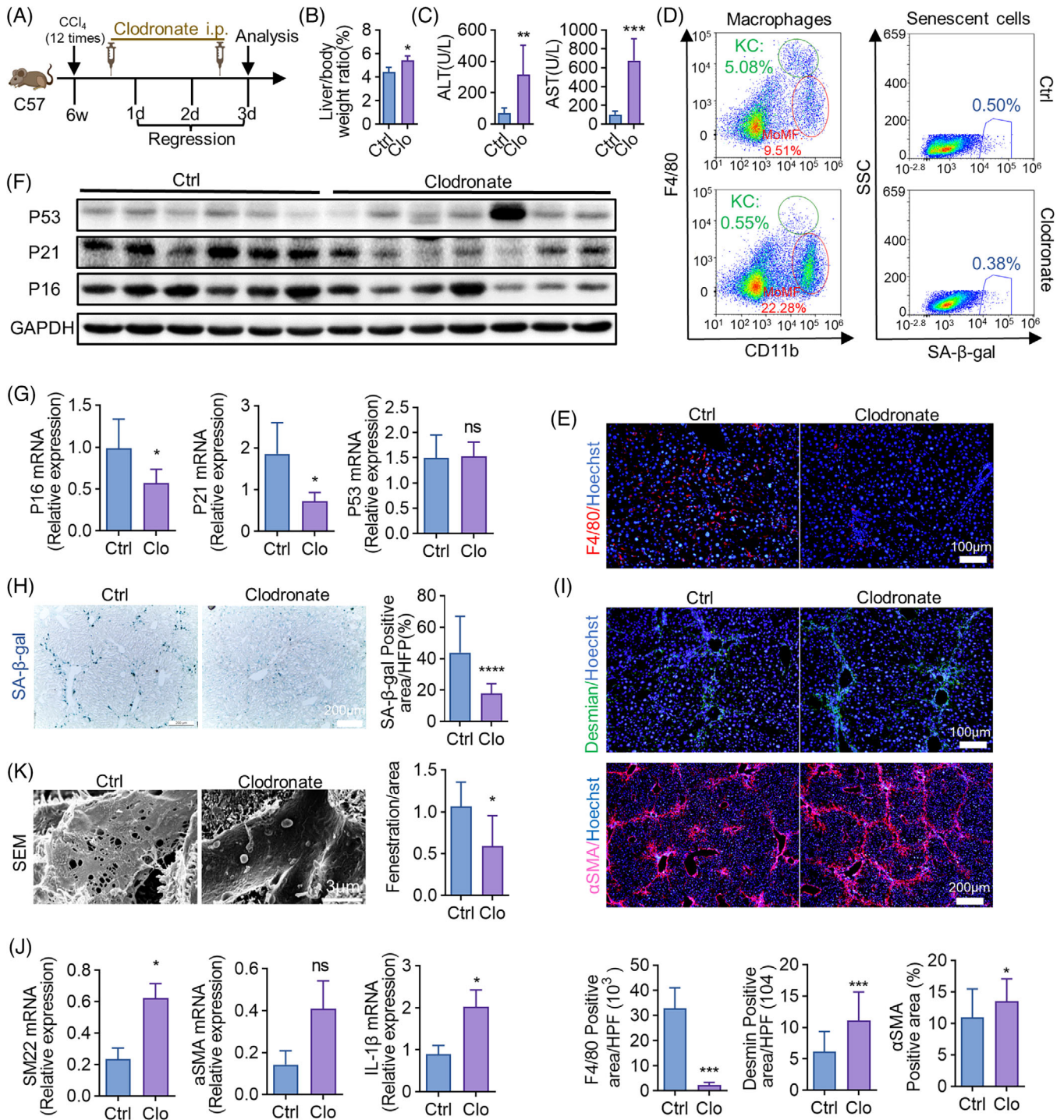


FIGURE 5 Depletion of macrophages alleviates cellular senescence and impedes liver fibrosis regression. (A) The strategy of clodronate liposome injection. All the experimental mice were sacrificed and analyzed on regression day 3. i.p. = intraperitoneal injection. (B) Liver to bodyweight ratios were measured in clodronate liposome-treated (Clo) and control mice. (C) Detection of serum ALT, AST levels in clodronate-treated and control mice. (D) The proportion of SA-β-gal⁺ and F4/80⁺ CD11b⁺ in liver NPCs of clodronate-treated and control mice was analyzed by FCM. (E) Anti-F4/80 IF staining of livers collected from clodronate-treated and control mice. F4/80-positive cells were quantitatively compared. Scale bar: 100 μm. (F) Protein levels of P16, P21, and P53 in livers of clodronate-treated and control mice were determined by WB; GAPDH served as an internal control. (G) The mRNA levels of P16, P21, and P53 were detected by RT-qPCR in clodronate-treated and control mice. (H) Staining of SA-β-gal. SA-β-gal-positive cells were quantitatively compared. Scale bar: 200 μm. (I) IF staining and quantification of desmin and αSMA in livers of clodronate-treated and control mice. Scale bar: 100 μm (desmin), scale bar: 200 μm (αSMA). (J) RT-qPCR analyses of mRNA expressions of SM22, αSMA, and IL-1β. (K) SEM analysis of liver sections collected from clodronate-treated and control mice. Sinusoidal fenestrae were quantitatively compared. Scale bar: 3 μm. Bars = means ± SD; n = 4–7; *p < 0.05, **p < 0.01, ***p < 0.001; ns, not significant.

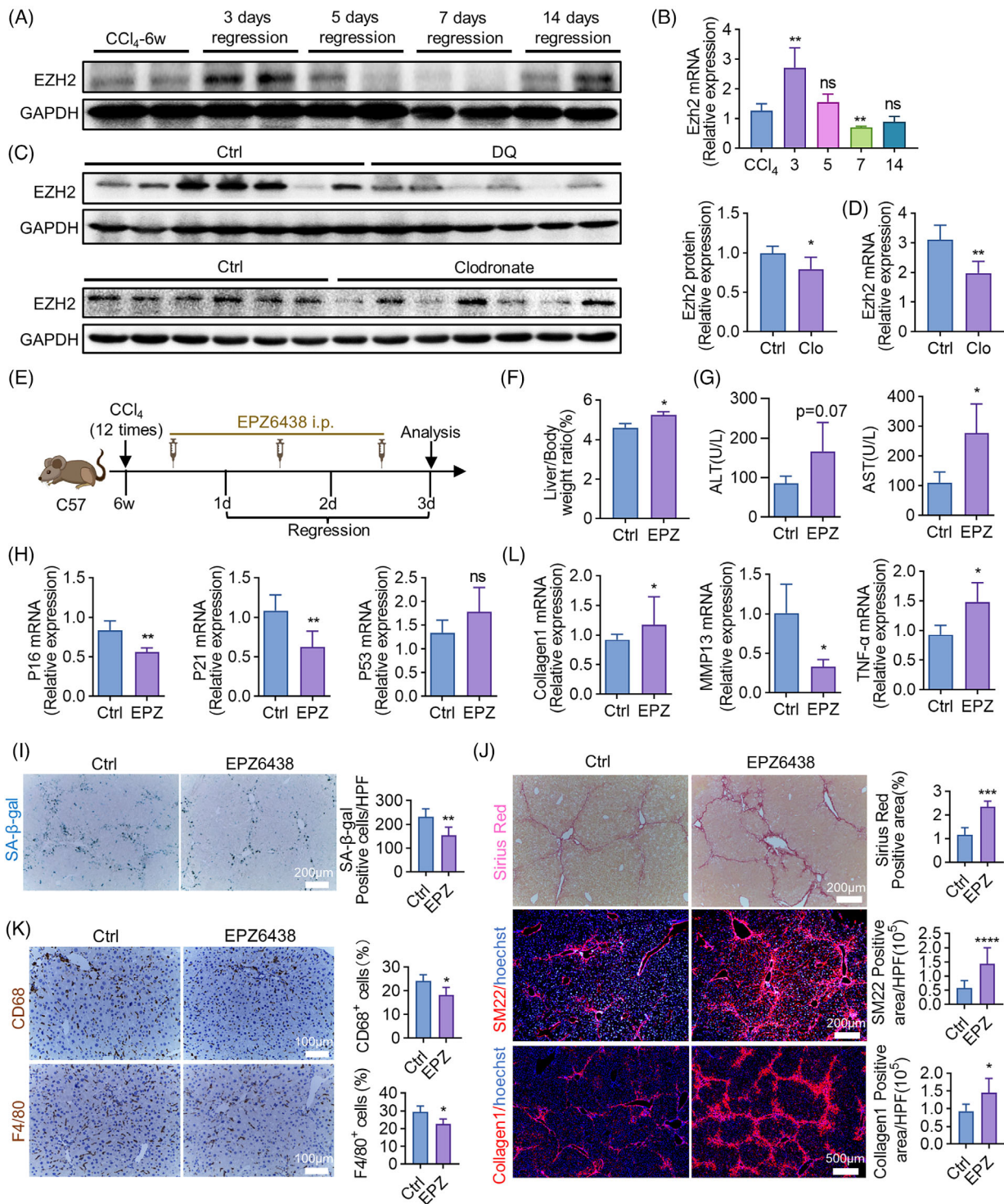


FIGURE 6 EZH2 promotes cellular senescence and liver fibrosis regression. (A and B) Protein (A) and mRNA (B) levels of EZH2 in isolated macrophages at various time points during liver fibrosis regression; GAPDH and β -actin served as internal controls. (C and D) Protein (C) and mRNA (D) levels of EZH2 in livers of DQ or clodronate-treated and control mice on regression day 3. GAPDH and β -actin served as internal controls. (E) The strategy of EPZ6438 administration. All the experimental mice were sacrificed and analyzed on regression day 3. (F) Liver to body weight ratios were detected in EPZ6438-treated (EPZ) and control mice. (G) Detection of serum ALT, AST. (H) The mRNA levels of P16, P21, and P53 were detected by RT-qPCR in EPZ6438-treated and control mice. (I) Staining of SA- β -gal. SA- β -gal-positive cells were quantitatively compared. Scale bar: 200 μ m. (J) Sirius red and IF staining (SM22, Collagen1) of livers of EPZ6438-treated and control mice. Positive areas were quantified and compared. Scale bar: 200 μ m (Sirius red, SM22), scale bar: 500 μ m (Collagen1). (K) Liver sections obtained from the EPZ6438-treated or control group were analyzed using immunohistochemical staining with anti-CD68 and anti-F4/80. Scale bar: 100 μ m. (L) RT-qPCR analyses of Collagen1, MMP13 (matrix metalloproteinase 13), and TNF- α (tumor necrosis factor α) in livers of EPZ6438-treated and control mice. Bars = means \pm SD; $n = 5$; * $p < 0.05$, ** $p < 0.01$, *** $p < 0.001$, **** $p < 0.0001$; ns, not significant.

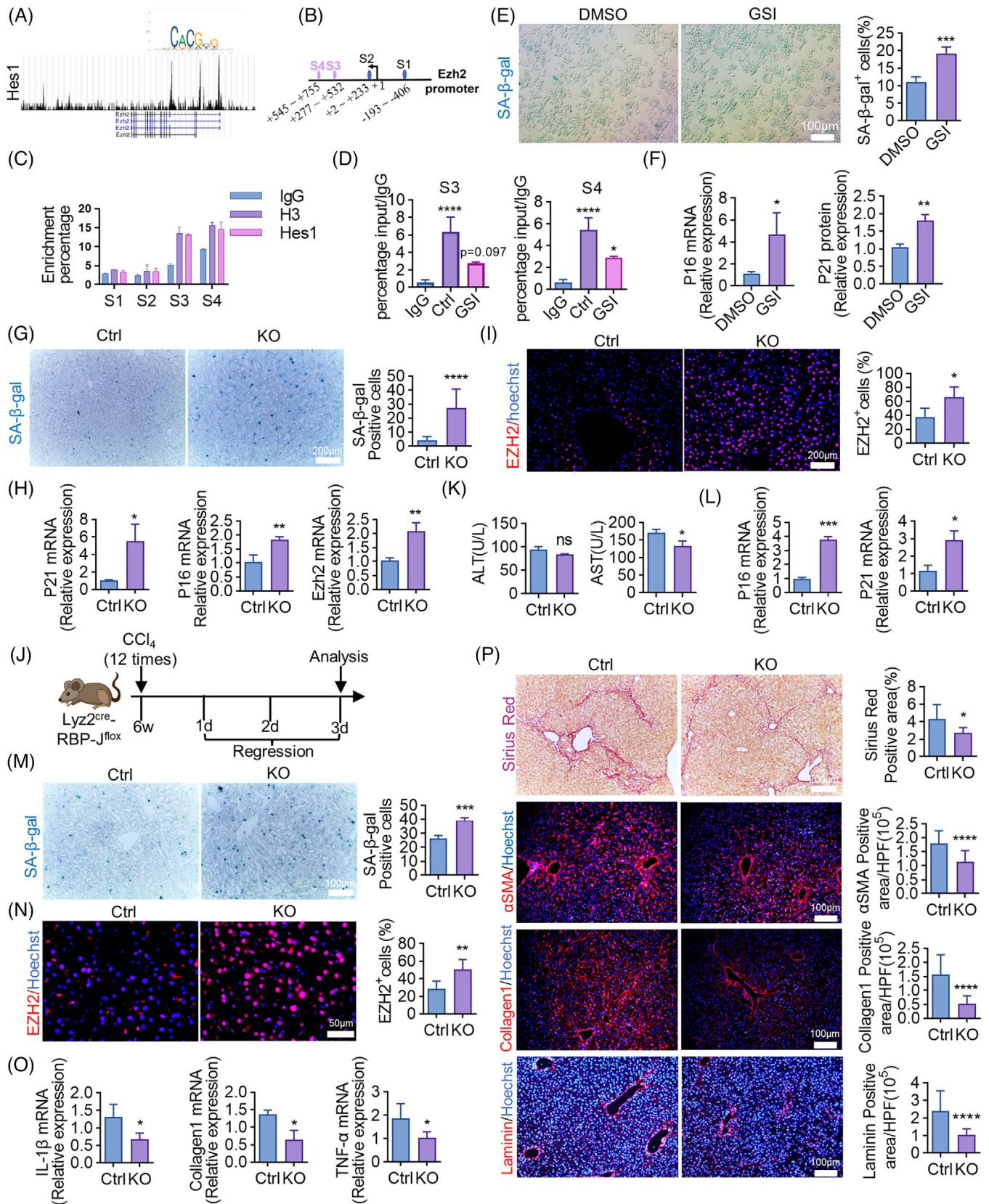


FIGURE 7 Notch-Hes1 impedes fibrosis regression by suppressing the transcription of EZH2. (A) Hes1 binding motif logo (<https://jaspar.genereg.net/analysis>). The relationship between promoter region of EZH2 and Hes1 was shown graphically by Cistrome Data Browser (<http://cistrome.org/db/#/>). (B) According to JASPAR database, EZH2 promoter region contains potential Hes1 binding sites. (C) Relative enrichment of EZH2 promoter sequences in control (IgG), positive control (H3), and Hes1 ChIPs in RAW264.7 cells. (D) Relative

not ALT level (Figure 7K). Meanwhile, aggravated hepatic cellular senescence, relieved fibrosis, and increased expression of EZH2 were detected in *Lyz2^{Cre}-RBP-J^{f/f}* mice (Figure 7L–P), proving Notch blockage in macrophages facilitated senescence-triggered fibrosis regression.

2.8 | Blocking EZH2 abrogates the increased senescence and accelerated fibrosis regression caused by Notch deficiency

To testify whether EZH2 blockage could reverse Notch deficiency-induced effects, EPZ6438 was adopted in *Lyz2^{Cre}-RBP-J^{f/f}* and control mice according to the strategy shown in Figure S2A. As expected, EPZ6438 largely restored the enhanced senescence, but deteriorated liver function in Notch-deficient mice (Figure S2B,C). Moreover, blocking EZH2 decelerated liver senescence and fibrosis regression in *Lyz2^{Cre}-RBP-J^{f/f}* mice (Figure S2D–F), suggesting that Notch counteracted senescence-driven fibrosis regression through regulating epigenetic EZH2 signaling.

2.9 | Notch inhibitor augments senescent cells and promotes fibrosis regression

To confirm the effect of Notch, LY3039478, another Notch inhibitor was administrated during the process of regression (Figure 8A). LY3039478, which recovered liver malfunction (Figure 8B), upregulated the expression of senescence-associated genes and inactivated Notch downstream gene *Hes1* (Figure 8C). Blocking Notch by LY3039478 stimulated hepatic cellular senescence and accelerated fibrosis regression (Figure 8D,E).

Previously, our group developed an exosome-mediated RBP-J decoy oligodeoxynucleotides (ODNs) (Figure 8F), which could be delivered to hepatic macrophages to ame-

liorate CCl₄-induced fibrosis by abrogating Notch/RBP-J signaling.⁴⁰ Thus, exosome-mediated RBP-J decoy was then manipulated to explore the therapeutic role of Notch in fibrosis regression (Figure 8G). RBP-J decoy reduced relative liver weight and serum ALT and AST levels (Figure 8H). To be noted, targeted delivery of exosome-mediated RBP-J decoy successfully stimulated senescence and fibrosis regression (Figure 8I). All these findings implied that targeting Notch signaling provided a potential way to promote fibrosis regression.

3 | DISCUSSION

Liver fibrosis due to viral, metabolic, or alcoholic chronic liver diseases is caused by excessive accumulation of extracellular matrix.⁴¹ Aggravated liver fibrosis leads to cirrhosis, portal hypertension, liver carcinoma, and liver failure, making a big challenge to global health.⁴² Thus, understanding the involved mechanisms of fibrogenesis is of great importance. Once the causative effects of chronic liver diseases cease, established fibrosis is reversible, which is called regression.⁴³ Growing studies have highlighted the importance of liver fibrosis regression,⁵ because it provides a promising therapeutic strategy to treat liver fibrosis.

In experimental investigations, the reversal of CCl₄-induced liver fibrosis could be detected in 1 or 2 weeks following the cessation of CCl₄ toxicity, which was usually determined by evaluation of fibrotic markers.⁴⁴ In this study, we observed that the regression of fibrosis initiated 3 days following the removal of CCl₄, as desmin and Masson stain significantly decreased at that time. Meanwhile, senescent cells accumulated in the recovered liver. The coincidence that the initiation of regression and emergence of senescence appeared at the same time aroused our great interests. To testify our hypothesis that the augmentation of senescent cells is the determinant of fibrosis regression, senescent cells were removed by

enrichment of EZH2 promoter sequences in control (IgG) and *Hes1* ChIPs in RAW264.7 cells treated with GSI. (E) RAW264.7 cells were cultured in vitro and stained by SA- β -gal. SA- β -gal-positive cells were quantitatively compared between GSI-treated and DMSO control groups. Scale bar: 100 μ m. (F) Relative mRNA expressions of P16 and P21 were determined in RAW264.7 cells treated with GSI or DMSO. (G) Liver sections collected from KO (*Lyz2^{Cre}-RBP-J^{f/f}*, homozygous) and control (*Lyz2^{Cre}-RBP-J^{f/+}*, heterozygous) mice were stained by SA- β -gal. SA- β -gal-positive cells were quantitatively compared. Scale bar: 200 μ m. (H) Relative mRNA expressions of P16, P21, and EZH2 were determined in KO and control mice. (I) IF staining of EZH2. EZH2-positive cells were quantitatively compared. Scale bar: 100 μ m. (J) The strategy of regression established in KO and control mice. All the experimental mice were sacrificed and analyzed on regression day 3. (K) Serum ALT, AST levels in KO and control mice. (L) Relative mRNA expressions of P16 and P21 were determined in KO and control mice. (M) SA- β -gal staining of livers of KO and control mice. SA- β -gal-positive cells were quantitatively compared. Scale bar: 100 μ m. (N) IF staining and quantification of EZH2 in livers of KO and control mice. Scale bar: 50 μ m. (O) Relative mRNA expressions of IL-1 β , Collagen1, TNF- α were determined in KO and control mice. (P) Sirius red, α SMA, Collagen1, and Laminin staining of livers of KO and control mice. Positive staining areas were quantitatively compared. Scale bar: 100 μ m (α SMA, Collagen1, Laminin), scale bar: 200 μ m (Sirius red).

Bars = means \pm SD; $n = 2-4$; * $p < 0.05$, ** $p < 0.01$, *** $p < 0.001$, **** $p < 0.0001$.

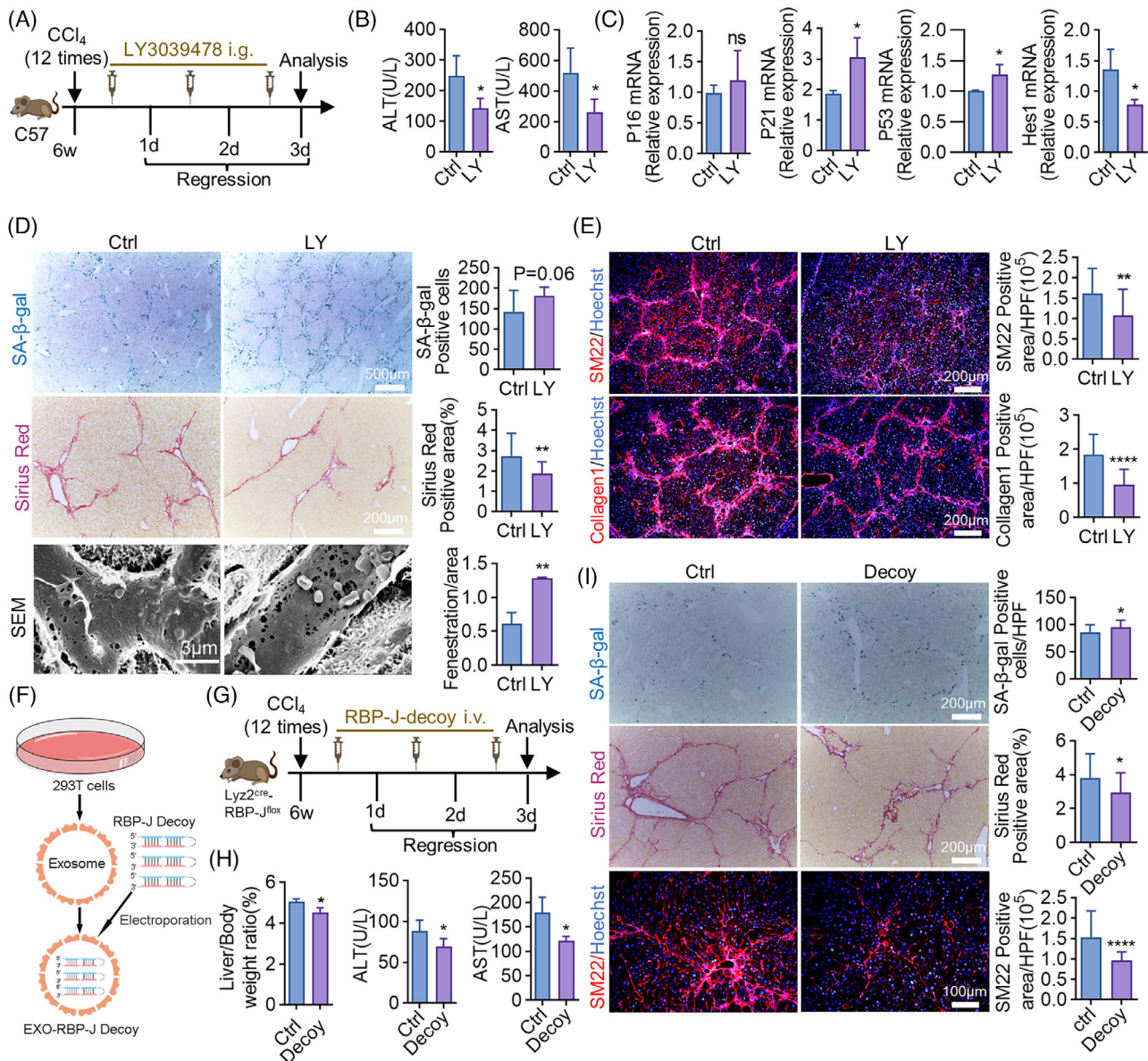


FIGURE 8 Blocking Notch signaling facilitates senescence-induced fibrosis regression. (A) The strategy of LY3039478 administration. All the experimental mice were sacrificed and analyzed on regression day 3. (B) Serum levels of ALT and AST in LY3039478-treated (LY) and control mice. (C) Relative mRNA levels of P16, P21, P53, and Hes1 were detected by RT-qPCR in LY3039478-treated or control mice. (D and E) Staining of SA-β-gal, Sirius red, SEM, Collagen1, and SM22 in mice subjected to LY3039478 treatment or not. Positive areas were quantified and compared. Scale bar: 500 μm (SA-β-gal), scale bar: 200 μm (Sirius red, SM22, Collagen1), scale bar: 3 μm (SEM). (F) Schematic representation of RBP-J decoy loaded into HEK293T-derived exosomes. (G) The strategy of the usage of exosome-mediated RBP-J decoy. All the experimental mice were sacrificed and analyzed on regression day 3. i.v. = intravenous injection. (H) Detection of liver/body weight, serum ALT, and AST in RBP-J decoy-treated (decoy) and control mice. (I) Staining of SA-β-gal, Sirius red, and SM22 in livers of RBP-J decoy-treated and control mice. SA-β-gal-positive cells, Sirius red and SM22 positive areas were quantitatively compared. Scale bar: 200 μm (SA-β-gal, Sirius red), scale bar: 100 μm (SM22). Bars = means ± SD; n = 4–5; *p < 0.05, **p < 0.01, ****p < 0.0001; ns, not significant.

senolytics. Interestingly, clearance of senescent cells after CCl₄ removal, deteriorated liver function and increased the expression of fibrotic markers, indicating that the regression of fibrosis was disturbed. Thus, we may conclude that the emerged senescent cells are beneficial to protect the injured liver against CCl₄ toxicity by advancing fibrosis regression.

After confirming the beneficial effect of senescence, the origin of senescent cells should be determined. Previously, Krizhanovsky et al. used IHC staining to show that senescent cells, which limited fibrogenesis, were activated stellated cells.¹⁵ In our study, FCM first identified that liver NPCs, particularly macrophages and endothelial cells, constituted the major proportion of senescent

cells. To confirm these findings, scRNA-seq was applied in livers of mice with CCl₄ removal. Although senescence-associated genes enriched in macrophages, endothelial cells, and myofibroblasts, the biggest alteration of P16 and P21, two landmark genes of senescence, was speculated in macrophages. IF staining also confirmed the co-stain of hepatic macrophages and senescence. In subsequent studies, either clearance of senescent cells or macrophages reduced hepatic senescent macrophages. Even if we could not conclude that senescent cells originated from macrophages, our findings illustrated that macrophages devoted great contribution to regression-related senescence. Recently, Satotaka et al. confirmed the existence of a cluster of P16^{high} hepatic senescent cells, which shared the expression of both endothelium and macrophage markers in fibrotic liver by scRNA-seq.⁴⁵ Thus, it seems to be extremely complicated to identify the constitution of fibrosis-associated senescent cells currently. Additionally, different injury models may lead to different cellular senescence during fibrosis. Our preliminary investigations suggested that non-alcoholic steatohepatitis (NASH)-associated fibrosis dominantly induced hepatocyte senescence; however, bile duct ligation-induced fibrosis probably triggered senescence of biliary epithelial cells.

The decisive role of macrophages in promoting inflammatory response during fibrogenesis has been extensively discussed.⁴⁶ In this study, a contradictory finding is that aggravated fibrosis was accompanied with decreased macrophages while senescent cells were removed. To elucidate this phenomenon, the polarization of macrophages was analyzed. Interestingly, the decrease of hepatic macrophages was due to the reduction of M2 macrophages, which mainly exerted anti-inflammatory effect.⁴⁷ Moreover, clearance of macrophages disrupted fibrosis regression as well, implying that depleted macrophages were predominantly anti-inflammatory ones. Therefore, emerged senescent cells may initiate liver fibrosis regression through igniting the anti-inflammatory attribute of macrophages.

As emerged senescence is beneficial to maintain fibrosis regression, stimulation of such senescence would be a protective way against liver fibrosis. In this study, the epigenetic modulator EZH2 was found to be transcriptionally suppressed by Notch-Hes1 signaling. Inactivation of Notch in transgenic mice facilitated fibrosis regression by augmenting EZH2-regulated senescence. For translational application, Ly3039478, a Notch inhibitor, was used to trigger senescence, which successfully accelerated fibrosis regression. However, the effect of Notch deficiency caused by Ly3039478 is global. Constructing a targeted delivery of Notch inhibitor to injured liver is an even better way to interfere fibrosis. RBP-J is the core transcriptional fac-

tor of Notch signaling pathway.⁴⁸ Previously, our group developed RBP-J decoy ODNs, which inactivated Notch signaling by suppressing RBP-J.⁴⁰ We found that injected exosome-equipped RBP-J decoy was mainly endocytosed by hepatic macrophages,⁴⁰ providing us with a promising strategy to target fibrotic liver. In this study, exosome-mediated RBP-J decoy promoted liver fibrosis regression by enhancing senescence. Thus, targeting Notch signaling provides an appealing strategy for the treatment of liver fibrosis.

Apart from regression, we also evaluated senescence during fibrosis progression. We found that senescent cells accumulated 1 week after CCl₄ administration (Figure S3A). Once macrophages were depleted at the beginning of fibrosis progression (Figure S3B), senescence was diminished and fibrosis was reversed (Figure S3C). Besides, removing senescent cells by DQ also alleviated CCl₄-induced fibrosis (Figure S4A–F). These data suggested that senescent cells probably play distinct roles in regulating progression and regression of liver fibrosis. To confirm this phenomenon, additional work should be carried out in the future. Besides, some other limitations are involved into this study. Precise identification of the origin of senescent cells should be considered in future work. Lineage tracing using P16 or P21-cre mice may provide a better way to distinguish which hepatic cells conducted senescence during regression. Although we presumably thought that senescent cells exerted M2 macrophage-like anti-inflammatory effects during regression, whether the polarization of hepatic macrophages changed after EZH2 or Notch disruption was not investigated in the current work. All these concerns need to be clarified in subsequent studies.

In conclusion, our study first unraveled that liver fibrosis regression was driven by macrophage senescence. Once anti-inflammatory senescent macrophages were abolished, fibrosis regression was terminated. Mechanistically, EZH2, which was transcriptionally impeded by Notch, strictly governed senescence-induced regression. Blocking Notch may treat fibrosis by augmenting EZH2-regulated senescence.

4 | MATERIALS AND METHODS

4.1 | Reagents

Dasatinib (SC0150) was purchased from Beyotime. Quercetin (S2391), DAPT (S2215), and LY3039478 (S7169) were purchased from Selleck. EPZ6438 (T1788) was purchased from Targetmol. Clodronate liposomes (40337ES10) were procured from Yeasen. The antibodies information used in the article is listed in Table S1.

4.2 | Mice

Male C57BL/6J mice (8 weeks old) were purchased from Charles River Laboratories. Mice of the C57BL/6 genetic background were bred in specific pathogen-free (SPF) facility. Lyz2-Cre mice (Jackson Laboratory, 004781) were crossed with RBP-J-flox mice.³⁹ Genomic DNA from the mouse tail was used as a template for PCR analysis of offspring genotypes.

To induce liver fibrosis, mice were intraperitoneally injected with olive oil or CCl₄ (0.6 μL/g, 15% with olive oil) for 6 weeks.⁴⁹ The regression of fibrosis was evaluated 3 days following the last injection of CCl₄. During the process of liver fibrosis, DQ (D: 5 mg/kg, Q: 50 mg/kg),⁵⁰ clodronate liposomes (50 mg/kg),⁵¹ LY3039478 (10 mg/kg),⁵² and EPZ6438 (34 mg/kg)⁵³ were used for specific experiments.

All animal experiments were performed in accordance with the principles approved by the Animal Experiment Administration Committee of the Fourth Military Medical University and with humanitarian care.

4.3 | Single-cell sequencing analysis

Single-cell RNA sequencing was performed with the assistance of Guangzhou Kidio Biotechnology, as we previously described.⁴⁹ GSVA analyses were carried out according to the published literature.⁵⁴

4.4 | Cell isolation

Isolation of mouse liver nonparenchymal cells was performed according to a two-step perfusion procedure described previously.⁵⁵ Anti-F4/80 and anti-CD146 magnetic beads were used for Kupffer cell and LSEC isolation, respectively.

4.5 | Fluorescent microsphere assay

Blood flow alterations were determined by injection of 15 μm fluorescent polystyrene microspheres (100 μL, F8842, Invitrogen) into the spleen. Determination of fluorescent microspheres was performed as described previously.¹⁹

4.6 | Chromatin immunoprecipitation assay

Chromatin immunoprecipitation assays were performed using the SimpleChIP Enzymatic Chromatin IP kit (CST,

9003) and anti-Hes1 antibody (CST, 11988) according to the manufacturer's instructions.¹⁹

4.7 | Exosomes loaded with RBP-J decoy oligodeoxynucleotides

4.7.1 | Extraction of exosomes from 293T cells

293T cells were overgrown with adherents, and the supernatant was collected after 48 h of culture with serum-free medium. The cell supernatant was centrifuged: 500 × g/5 min, 3000 × g/30 min, and the supernatant was incubated with PEG6000 overnight. The next day, the supernatant incubated overnight with PEG6000 was centrifuged at 12,000 × g/1 h. The supernatant was discarded, and the precipitate (exosomes) was resuspended with an appropriate amount of sterile PBS.

4.7.2 | Electroporation

The nucleic acid sequence of the RBP-J decoy ODNs (decoy RBP-J) was 5'-CTGCGTGGGAACCTA GCGTGGGAATATTTTTATATTCCCACGCTAGTTCCC ACGCAG-3'; the nucleic acid sequence of the control decoy ODNs (decoy Ctrl) was 5'-CTGCGTTTTAACTAGCGTTTTAATTTTTATATTAA AACGCTAGTTAAAACGCAG-3'.⁴⁰ Two RBP-J binding sites (CGTGGGAA) were present in the decoy, with three phosphorothioate-modified sites at each end.⁴⁰ All the ODNs were synthesized exclusively by Tsingke Biotechnology Co. (Beijing, China). Each mouse was mixed with RBPJ-Decoy/control decoy ODNs (2.5 nmol) and exosomes (BCA quantification of 200 μg) in a 0.4 cm electric piercing cup (Bio-Rad), supplemented with a certain amount of electric piercing buffer (Bio-Rad), electroporated with 400 V and 125 μF. Rewarming in the incubator at 37°C for 30 min. After mixing the liquid in the electric perforator cup with one-third volume of PEG6000, centrifugation performed at 12,000 × g/15 min. The discarded supernatant was resuspended with sterile PBS.

4.7.3 | Exosome injection

Exosomes containing RBPJ/control decoy ODNs were administered intravenously via the tail vein for three times per 3 days when 3 days after ablation in liver fibrosis model. Mice were euthanased after 3 days of CCl₄ withdrawal for further experiments.

4.8 | Senescence-associated β -galactosidase staining

Senescence was assessed by staining 8–10 μm frozen sections of mouse liver¹⁹ using Senescence β -Galactosidase Staining Kit (Beyotime, C0602), according to the manufacturer's instructions.

4.9 | Flow cytometry

The flow cytometry analysis was conducted in accordance with the previously established protocol.⁵⁶ An overview of antibody information can be found in Table S1.

4.10 | Apoptosis assay

Cell apoptosis was assessed via TUNEL assay utilizing the One Step TUNEL Apoptosis Assay Kit (Beyotime, C1089). Refer to the manufacturer's guidelines for comprehensive staining protocols.

4.11 | Scanning electron microscopy

The scanning electron microscopy was conducted in accordance with the previously established protocol.⁴⁸

4.12 | Real-time quantitative PCR assay

Total RNA from primary macrophages or liver tissues was harvested in Trizol reagent. Evo M-MLV RT Kit (Accurate Biology, AG11728) was employed to synthesize cDNA. The SYBR Green PCR Master Mix (Accurate Biology, AG11701) was utilized for performing RT-qPCR analysis using the Bio Rad C1000 Touch instrument. Actin was utilized to normalize the RT-qPCR data. The primer pairs used in this article are listed in Table S2.

4.13 | Western blot analysis

Liver tissues or macrophages were lysed with RAPI. Subsequently, the mixture was treated with grinding plus ultrasonic crushing. After being centrifuged, the supernatant was removed and incubated for 10 min at 100°C with 5 \times SDS. The BCA protein quantification kit (Thermo Fisher Scientific) was used to determine protein content. SDS-polyacrylamide gel electrophoresis was used to separate equal amounts of protein, which was then trans-

ferred to PVDF membranes. After 5% milk blocking, the primary antibody and corresponding secondary antibody were incubated (antibody information refers to Table S1), and finally the protein band was exposed with an instrument. The protein signals were captured by the Chemi Doc XRS+ System (Bio-Rad Laboratories, Inc.), followed by the analyses using the ImageJ software.

4.14 | Histological staining

The perfused liver was soaked in 4% paraformaldehyde for 4–12 h. A frozen section was made by dehydrating tissue in 30% sucrose overnight, embedding it in OCT, and sectioning it at 8–10 μm . Immunofluorescence (IF) and immunohistochemistry (IHC) staining were completed as previously described conducted.⁵⁵ The statistical methods for the images of IHC were the number of α -SMA, Sirius Red and Collagen1-positive pixels (SUM value output in the software)/the resolution of the Image (2048 \times 1536) \times 100%. An overview of antibody information can be found in Table S1.

4.15 | Statistical analysis

GraphPad Prism was used for statistical analysis, and data were reported as mean \pm SD. An unpaired *t*-test (Student's *t*-test) was used to make group comparisons. *p*-Values < 0.05 were considered as a measure of statistical significance. **p* < 0.05, ***p* < 0.01, ****p* < 0.001, *****p* < 0.0001; ns, not significant.

AUTHOR CONTRIBUTORS

PS, JLD, and JD conducted the experiments. JLL, ZQF, HX, ZWL, and WD provided assistance in animal experimentation. MX, YWL, and FH aided in data collection. KST and LW developed the experimental design. LW authored the article. All authors have read and approved the final manuscript.

ACKNOWLEDGMENTS

We express our gratitude to Professor Hua Han from Fourth Military Medical University for his invaluable technical support.

CONFLICT OF INTEREST STATEMENT

The authors declare that they have no conflicts of interest.

DATA AVAILABILITY STATEMENT

The data utilized in this study can be made available upon request from the corresponding author.

ETHICS APPROVAL

The Animal Experiment Administration Committee of the Fourth Military Medical University reviewed and approved all animal experiments to ensure ethical and humane treatment of animals (KY20223331-1).

ORCID

Lin Wang  <https://orcid.org/0000-0001-5586-3012>

REFERENCES

- Kisseleva T, Brenner D. Molecular and cellular mechanisms of liver fibrosis and its regression. *Nat Rev Gastroenterol Hepatol*. 2021;18(3):151-166.
- Ellis EL, Mann DA. Clinical evidence for the regression of liver fibrosis. *J Hepatol*. 2012;56(5):1171-1180.
- Poisson J, Lemoine S, Boulanger C, et al. Liver sinusoidal endothelial cells: physiology and role in liver diseases. *J Hepatol*. 2017;66(1):212-227.
- Zhang CY, Yuan WG, He P, Lei JH, Wang CX. Liver fibrosis and hepatic stellate cells: etiology, pathological hallmarks and therapeutic targets. *World J Gastroenterol*. 2016;22(48):10512-10522.
- Campana L, Iredale JP. Regression of liver fibrosis. *Semin Liver Dis*. 2017;37(1):1-10. doi:10.1055/s-0036-1597816
- Parola M, Pinzani M. Liver fibrosis: pathophysiology, pathogenetic targets and clinical issues. *Mol Aspects Med*. 2019;65:37-55.
- Friedman SL, Pinzani M. Hepatic fibrosis 2022: unmet needs and a blueprint for the future. *Hepatology*. 2022;75(2):473-488.
- Hernandez-Segura A, Nehme J, Demaria M. Hallmarks of cellular senescence. *Trends Cell Biol*. 2018;28(6):436-453.
- Serrano M, Lin AW, McCurrach ME, Beach D, Lowe SW. Oncogenic ras provokes premature cell senescence associated with accumulation of p53 and p16INK4a. *Cell*. 1997;88(5):593-602.
- van Deursen JM. The role of senescent cells in ageing. *Nature*. 2014;509(7501):439-446.
- Campisi J. Senescent cells, tumor suppression, and organismal aging: good citizens, bad neighbors. *Cell*. 2005;120(4):513-522.
- Muñoz-Espín D, Serrano M. Cellular senescence: from physiology to pathology. *Nat Rev Mol Cell Biol*. 2014;15(7):482-496.
- He S, Sharpless NE. Senescence in health and disease. *Cell*. 2017;169(6):1000-1011.
- Regulski MJ. Cellular senescence: what, why, and how. *Wounds*. 2017;29(6):168-174.
- Krizhanovsky V, Yon M, Dickins RA, et al. Senescence of activated stellate cells limits liver fibrosis. *Cell*. 2008;134(4):657-667.
- Grosse L, Wagner N, Emelyanov A, et al. Defined p16(high) senescent cell types are indispensable for mouse healthspan. *Cell Metab*. 2020;32(1):87-99.
- Papatheodoridi AM, Chrysavgis L, Koutsilieris M, Chatzigeorgiou A. The role of senescence in the development of nonalcoholic fatty liver disease and progression to nonalcoholic steatohepatitis. *Hepatology*. 2020;71(1):363-374.
- Martel J, Ojcius DM, Wu CY, et al. Emerging use of senolytics and senomorphics against aging and chronic diseases. *Med Res Rev*. 2020;40(6):2114-2131.
- Duan JL, Ruan B, Song P, et al. Shear stress-induced cellular senescence blunts liver regeneration through Notch-sirtuin 1-P21/P16 axis. *Hepatology*. 2022;75(3):584-599.
- Zhou X, Xiong C, Tolbert E, et al. Targeting histone methyltransferase enhancer of zeste homolog-2 inhibits renal epithelial-mesenchymal transition and attenuates renal fibrosis. *Faseb J*. 2018;32(11):fj201800237R.
- Gan L, Yang Y, Li Q, et al. Epigenetic regulation of cancer progression by EZH2: from biological insights to therapeutic potential. *Biomark Res*. 2018;6:10.
- Wei FZ, Cao Z, Wang X, et al. Epigenetic regulation of autophagy by the methyltransferase EZH2 through an MTOR-dependent pathway. *Autophagy*. 2015;11(12):2309-2322.
- Wu ZL, Zheng SS, Li ZM, et al. Polycomb protein EZH2 regulates E2F1-dependent apoptosis through epigenetically modulating Bim expression. *Cell Death Differ*. 2010;17(5):801-810.
- Wu Z, Lee ST, Qiao Y, et al. Polycomb protein EZH2 regulates cancer cell fate decision in response to DNA damage. *Cell Death Differ*. 2011;18(11):1771-1779.
- Lim HJ, Kim M. EZH2 as a potential target for NAFLD therapy. *Int J Mol Sci*. 2020;21(22):8617.
- Duan R, Du W, Guo W. EZH2: a novel target for cancer treatment. *J Hematol Oncol*. 2020;13(1):104.
- Zhou L, Mudianto T, Ma X, Riley R, Uppaluri R. Targeting EZH2 enhances antigen presentation, antitumor immunity, and circumvents anti-PD-1 resistance in head and neck cancer. *Clin Cancer Res*. 2020;26(1):290-300.
- Paredes S, Angulo-Ibanez M, Tasselli L, et al. The epigenetic regulator SIRT7 guards against mammalian cellular senescence induced by ribosomal DNA instability. *J Biol Chem*. 2018;293(28):11242-11250.
- Milanovic M, Fan DNY, Belenki D, et al. Senescence-associated reprogramming promotes cancer stemness. *Nature*. 2018;553(7686):96-100.
- Sha MQ, Zhao XL, Li L, et al. EZH2 mediates lidamycin-induced cellular senescence through regulating p21 expression in human colon cancer cells. *Cell Death Dis*. 2016;7(11):e2486.
- Rani A, Greenlaw R, Smith RA, Galustian C. HES1 in immunity and cancer. *Cytokine Growth Factor Rev*. 2016;30:113-117.
- Vasyutina E, Lenhard DC, Wende H, et al. RBP-J (Rbpsi) is essential to maintain muscle progenitor cells and to generate satellite cells. *Proc Natl Acad Sci U S A*. 2007;104(11):4443-4448.
- Richter ML, Deligiannis IK, Yin K, et al. Single-nucleus RNA-seq2 reveals functional crosstalk between liver zonation and ploidy. *Nat Commun*. 2021;12(1):4264.
- Kusumoto D, Seki T, Sawada H, et al. Anti-senescent drug screening by deep learning-based morphology senescence scoring. *Nat Commun*. 2021;12(1):257.
- Kirkland JL, Tchkonina T. Senolytic drugs: from discovery to translation. *J Intern Med*. 2020;288(5):518-536.
- Pradere JP, Kluwe J, De Minicis S, et al. Hepatic macrophages but not dendritic cells contribute to liver fibrosis by promoting the survival of activated hepatic stellate cells in mice. *Hepatology*. 2013;58(4):1461-1473.
- Lee WJ, Tateya S, Cheng AM, et al. M2 macrophage polarization mediates anti-inflammatory effects of endothelial nitric oxide signaling. *Diabetes*. 2015;64(8):2836-2846.
- Zheng Z, Wang H, Li L, et al. Splenectomy enhances the Ly6C(low) phenotype in hepatic macrophages by activating the ERK1/2 pathway during liver fibrosis. *Int Immunopharmacol*. 2020;86:106762.

39. Ma J, Liu Y-L, Hu Y-Y, et al. Disruption of the transcription factor RBP-J results in osteopenia attributable to attenuated osteoclast differentiation. *Mol Biol Rep.* 2013;40(3):2097-2105.
40. He F, Li WN, Li XX, et al. Exosome-mediated delivery of RBP-J decoy oligodeoxynucleotides ameliorates hepatic fibrosis in mice. *Theranostics.* 2022;12(4):1816-1828.
41. Delgado ME, Cárdenas BI, Farran N, Fernandez M. Metabolic reprogramming of liver fibrosis. *Cells.* 2021;10(12):3604.
42. Osná NA, Donohue TM Jr, Kharbanda KK. Alcoholic liver disease: pathogenesis and current management. *Alcohol Res.* 2017;38(2):147-161.
43. Dhar D, Baglieri J, Kisseleva T, Brenner DA. Mechanisms of liver fibrosis and its role in liver cancer. *Exp Biol Med (Maywood).* 2020;245(2):96-108.
44. Ramachandran P, Pellicoro A, Vernon MA, et al. Differential Ly-6C expression identifies the recruited macrophage phenotype, which orchestrates the regression of murine liver fibrosis. *Proc Natl Acad Sci U S A.* 2012;109(46):E3186-E3195.
45. Omori S, Wang TW, Johmura Y, et al. Generation of a p16 reporter mouse and its use to characterize and target p16(high) cells in vivo. *Cell Metab.* 2020;32(5):814-828.
46. Wynn TA, Barron L. Macrophages: master regulators of inflammation and fibrosis. *Semin Liver Dis.* 2010;30(3):245-257.
47. Ye L, He S, Mao X, et al. Effect of hepatic macrophage polarization and apoptosis on liver ischemia and reperfusion injury during liver transplantation. *Front Immunol.* 2020;11:1193.
48. Dou GR, Wang YC, Hu XB, et al. RBP-J, the transcription factor downstream of Notch receptors, is essential for the maintenance of vascular homeostasis in adult mice. *Faseb J.* 2008;22(5):1606-1617.
49. Ruan B, Duan JL, Xu H, et al. Capillarized liver sinusoidal endothelial cells undergo partial endothelial-mesenchymal transition to actively deposit sinusoidal ECM in liver fibrosis. *Front Cell Dev Biol.* 2021;9:671081.
50. Xu M, Pirtskhalava T, Farr JN, et al. Senolytics improve physical function and increase lifespan in old age. *Nat Med.* 2018;24(8):1246-1256.
51. Piaggio F, Kondylis V, Pastorino F, et al. A novel liposomal Clodronate depletes tumor-associated macrophages in primary and metastatic melanoma: anti-angiogenic and anti-tumor effects. *J Control Release.* 2016;223:165-177.
52. Fang ZQ, Ruan B, Liu JJ, et al. Notch-triggered maladaptation of liver sinusoidal endothelium aggravates nonalcoholic steatohepatitis through endothelial nitric oxide synthase. *Hepatology.* 2022;76(3):742-758.
53. Duan D, Shang M, Han Y, et al. EZH2-CCF-cGAS axis promotes breast cancer metastasis. *Int J Mol Sci.* 2022;23(3):1788.
54. Crespo-García S, Tsuruda PR, Dejda A, et al. Pathological angiogenesis in retinopathy engages cellular senescence and is amenable to therapeutic elimination via BCL-xL inhibition. *Cell Metab.* 2021;33(4):818-832.
55. Duan JL, Ruan B, Yan XC, et al. Endothelial Notch activation reshapes the angiocrine of sinusoidal endothelia to aggravate liver fibrosis and blunt regeneration in mice. *Hepatology.* 2018;68(2):677-690.
56. Duan JL, Zhou ZY, Ruan B, et al. Notch-regulated c-kit-positive liver sinusoidal endothelial cells contribute to liver zonation and regeneration. *Cell Mol Gastroenterol Hepatol.* 2022;13(6):1741-1756.

SUPPORTING INFORMATION

Additional supporting information can be found online in the Supporting Information section at the end of this article.

How to cite this article: Song P, Duan J, Ding J, et al. Cellular senescence primes liver fibrosis regression through Notch-EZH2. *MedComm.* 2023;4:e346. <https://doi.org/10.1002/mco2.346>